

Lanthanide-Nucleotide Coordination Nanoparticles for STING Activation

Zichao Luo,¹ Xiuqi Liang,¹ Tao He, Xian Qin, Xinchao Li, Yueshan Li, Lu Li, Xian Jun Loh, Changyang Gong,* and Xiaogang Liu*



Cite This: *J. Am. Chem. Soc.* 2022, 144, 16366–16377



Read Online

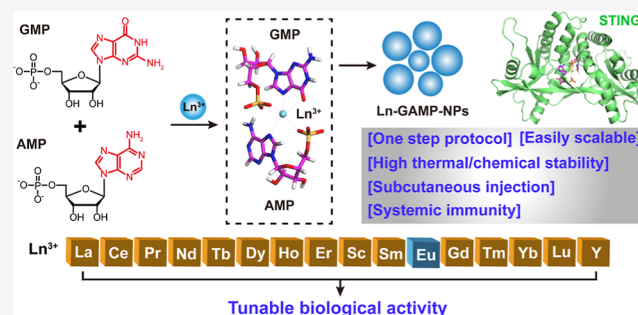
ACCESS |

Metrics & More

Article Recommendations

Supporting Information

ABSTRACT: Activation of the stimulator of interferon genes (STING) is essential for blocking viral infections and eliciting antitumor immune responses. Local injection of synthetic STING agonists, such as 2′3′-cGAMP [cGAMP = cyclic 5′-guanosine monophosphate (cGMP)–adenosine monophosphate (AMP)], is a promising approach to enhance antiviral functions and cancer immunotherapy. However, the application of such agonists has been hindered by complicated synthetic procedures, high doses, and unsatisfactory systemic immune responses. Herein, we report the design and synthesis of a series of 2′3′-cGAMP surrogates in nanoparticle formulations formed by reactions of AMP, GMP, and coordinating lanthanides. These nanoparticles can stimulate the



type-I interferon (IFN) response in both mouse macrophages and human monocytes. We further demonstrate that the use of europium-based nanoparticles as STING-targeted adjuvants significantly promotes the maturation of mouse bone-marrow-derived dendritic cells and major histocompatibility complex class I antigen presentation. Dynamic molecular docking analysis revealed that these nanoparticles bind with high affinity to mouse STING and human STING. Compared with soluble ovalbumin (OVA), subcutaneously immunized europium-based nanovaccines exhibit significantly increased production of primary and secondary anti-OVA antibodies (~180-fold) in serum, as well as IL-5 (~28-fold), IFN- γ (~27-fold), and IFN- α/β (~4-fold) in splenocytes ex vivo. Compared with the 2′3′-cGAMP/OVA formulation, subcutaneous administration of nanovaccines significantly inhibits B16F10-OVA tumor growth and prolongs the survival of tumor-bearing mice in both therapeutic and protective models. Given the rich supramolecular chemistry with lanthanides, this work will enable a readily accessible platform for potent humoral and cellular immunity while opening new avenues for cost-effective, highly efficient therapeutic delivery of STING agonists.

INTRODUCTION

The stimulator of interferon genes (STING), a signaling molecule localized in the endoplasmic reticulum (ER), is essential for the spontaneous induction of antitumor T-cell immunity by regulating the transcription of many host defense genes, such as pro-inflammatory cytokines and type-I interferons (IFN-I).^{1–3} The STING pathway is activated by cyclic dinucleotides (CDNs) such as 2′3′-cGAMP [cGAMP = cyclic 5′-guanosine monophosphate (cGMP)–adenosine monophosphate (AMP)].⁴ Upon stimulation by CDNs, the STING pathway then initiates TANK-binding kinase 1 (TBK1) and interferon regulatory factor 3 (IRF3), which promote the production of pro-inflammatory cytokines and IFN- α/β , respectively.⁵ These cytokines and IFN-I activate dendritic cells (DCs), attract natural killer (NK) cells to the tumor, and present tumor antigens for subsequent initiation of anti-tumor T cells.⁶

CDN-mediated STING activation has made great strides in inhibiting the growth of solid and hematological tumors via various mechanisms of immune activation, such as the

expansion and activation of CD8⁺ T cells or the accumulation of macrophages in tumor tissues.^{7,8} However, these CDN-mediated therapeutic effects are limited by their low bioavailability and poor cellular permeability, which are due to their anionic and highly water-soluble characteristics.^{9,10} In addition, to achieve adequate biological activity, CDNs are usually used at relatively high concentrations, necessitating frequent injections into the tumor.^{7,11} However, excessive concentrations of intra-tumoral CDNs may promote tumor growth and increase the risk of metastasis by inducing overexpression of programmed death-ligand 1 (PD-L1) on tumor cells,^{12–14} recruiting tumor-infiltrating regulatory T cells

Received: March 27, 2022

Published: August 29, 2022



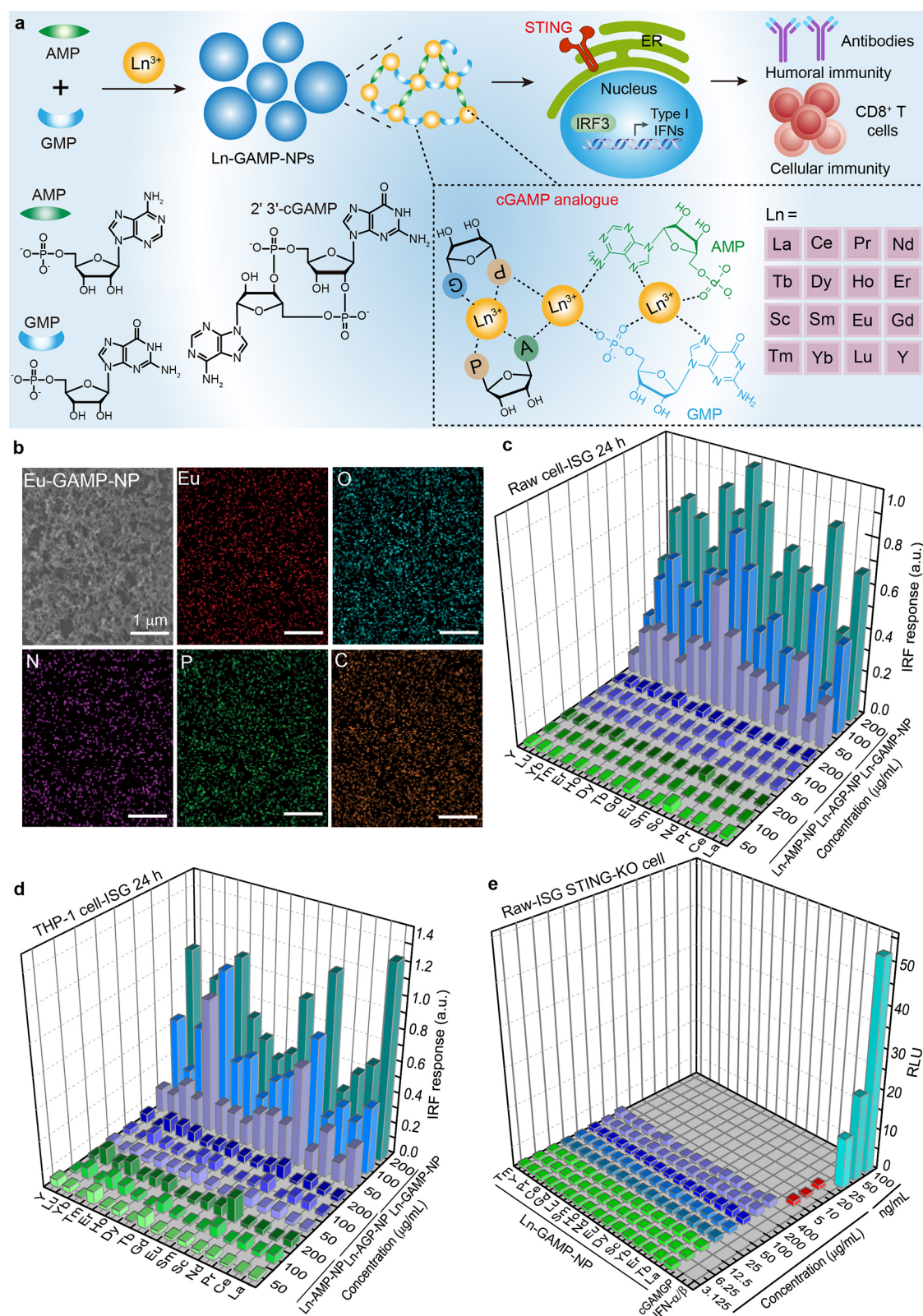


Figure 1. Design of lanthanide-based coordination nanoparticles to induce IRF responses in Raw IFN-stimulated gene (ISG) and THP-1 ISG cells. (a) Schematic design of a lanthanide-based cGAMP surrogate for STING activation. (b) Scanning electron microscopy images and elemental mapping of Eu-GAMP-NPs. Scale bar, 1 μm . (c,d) IRF responses of Raw ISG and THP-1 ISG cells treated with Ln-GMP-NPs, Ln-AMP-NPs, or Ln-GAMP-NPs for 24 h. (e) Relative light units (RLU) of Ln-GAMP-NPs, cGAMP, or IFN- α/β in Raw-ISG STING-KO cells. Data are averages of three independent experiments.

(Tregs) to the tumor¹⁵ or disrupting the tumor microenvironment and vascular networks.^{12,16}

To overcome the above limitations, one strategy is to use nanoparticles as carriers to deliver STING agonists to tumor

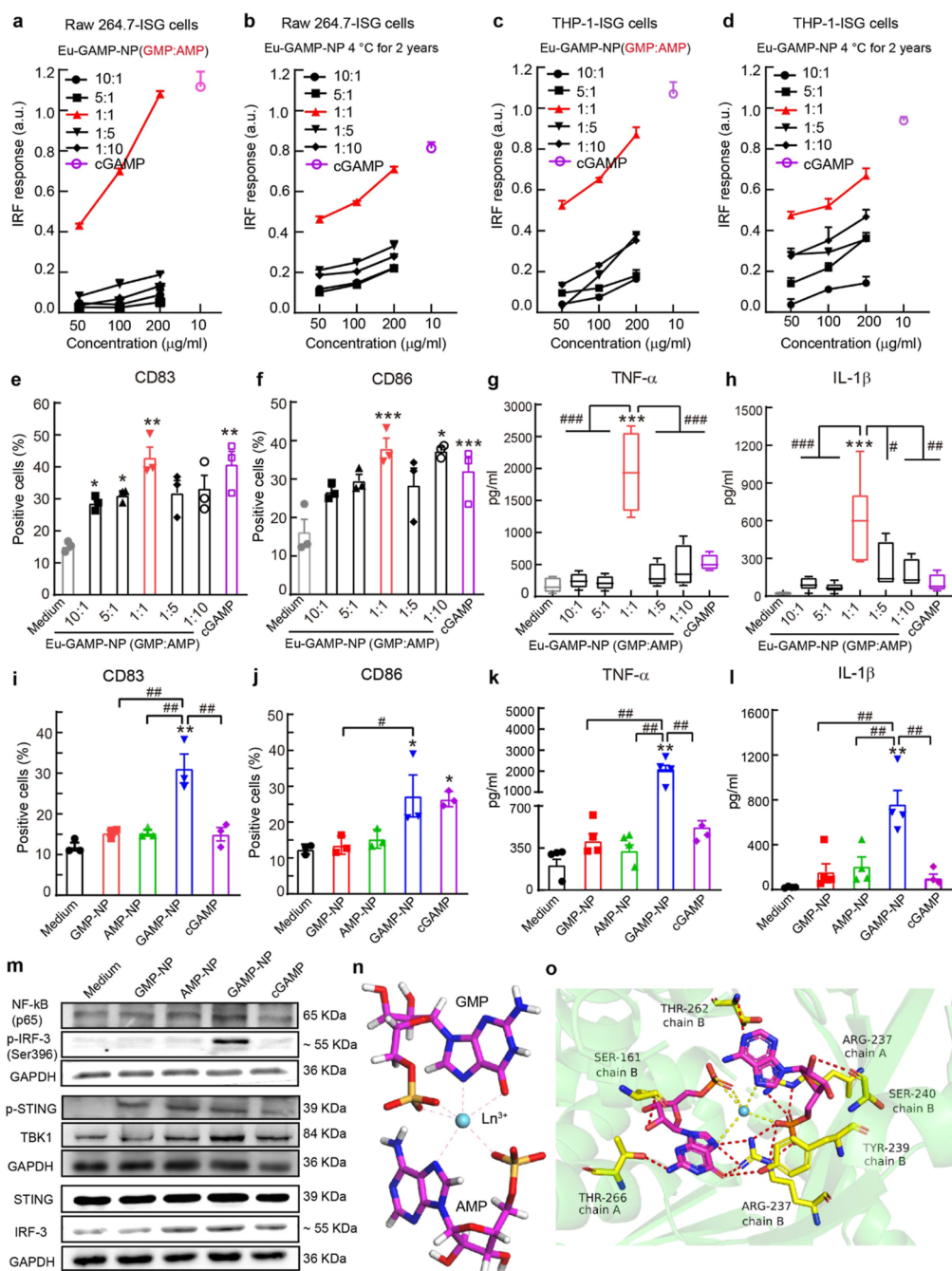


Figure 2. Eu-GAMP-NPs induce maturation of BMDCs via the STING pathway. (a,b) IRF responses of Raw ISG cells treated with Eu-GAMP-NPs (a) at different molar ratios of GMP/AMP and (b) after storage at 4 °C for over 2 years. (c,d) IRF responses of THP-1 ISG cells treated with Eu-GAMP-NPs (c) prepared in various molar ratios of GMP/AMP and (d) after storage at 4 °C for over 2 years. (e,f) Expression of CD83 and CD86, respectively, on BMDCs treated with Eu-GAMP-NPs for 24 h. (g,h) Production of TNF- α and IL-1 β by BMDCs incubated with Eu-GAMP-NPs for 24 h. (i,j) Effect of Eu-GMP-NPs, Eu-AMP-NPs, or Eu-GAMP-NPs on CD83 or CD86 expression by BMDCs. (k,l) Effect of Eu-GMP-NPs, Eu-AMP-NPs, or Eu-GAMP-NPs on TNF- α and IL-1 β production by BMDCs. (m) Western blotting analysis of the STING pathway. (n) Calculated molecular structure of Ln-GAMP-NPs shown as sticks and colored by atom type (C, purple; O, red; N, blue; H, white; and P, yellow). (o) Intermolecular contacts and hydrogen bonding associated with binding of Ln-GAMP-NPs to mouse STING^{R231} (PDB ID 4LOK, ref 26). Dashed red lines represent hydrogen bonds between Ln-GAMP-NPs and residues of mSTING. Yellow-purple and reddish-blue sticks represent residues of individual monomers of the mSTING^{R231} dimer and Ln-GAMP-NPs, respectively. The dashed yellow lines represent interactions between lanthanide ions and nucleotide molecules. Values are means \pm s.e.m. ($n = 3-4$ biologically independent samples; asterisks: Medium vs other treatments, * $P < 0.05$; ** $P < 0.01$; *** $P < 0.001$; hash: two different groups, # $P < 0.05$; ## $P < 0.01$; ### $P < 0.001$; one-way ANOVA with Tukey's test).

sites. Various nanoparticles, such as pH-responsive polymerosomes,¹⁰ liposomes,¹⁷ polylactic-*co*-glycolic acid (PLGA) microparticles,¹³ or mesoporous silica nanoparticles,¹⁸ have been used for the delivery of 2', 3'-cGAMP, a classic small-

molecule STING agonist, with improved therapeutic efficacy. Apart from side effects caused by intratumoral injection, the complex process of nanoparticle synthesis and encapsulation of the STING agonist may limit its application. To circumvent

the contraindications of intratumoral injection, small-molecule or polymeric STING agonists have been developed to elicit systemic anti-tumor activity by oral, subcutaneous, or intraperitoneal administration.^{19–21} These agonists significantly inhibited tumor growth in various tumor models when used as antitumor drugs or protein/mRNA vaccines. However, there are challenges in the large-scale application of these STING agonists due to the complexity of nanoparticle processing and early screening and identification of small-molecule STING agonists.

Herein, we have designed a series of simple robust STING-activating coordination nanoparticles by coordinating lanthanide ions with disodium GMP and AMP. We found that 16 lanthanide ions could be formed into coordination nanoparticles (Ln-GAMP-NPs). All of these Ln-GAMP-NPs activate the STING signaling pathway in mouse macrophages and human monocytes. Europium-based coordination nanoparticles (Eu-GAMP-NPs) were randomly selected to evaluate their adjuvant effects *in vitro* and *in vivo*. The data show that Eu-GAMP-NPs induce the maturation of bone-marrow-derived dendritic cells (BMDCs) via the STING signaling pathway and promote antigen cross-presentation via the major histocompatibility complex (MHC)-I pathway. After subcutaneous injection, the Eu-GAMP-NP-based vaccine significantly enhanced both humoral and cellular immune responses associated with the STING pathway, as shown by the increase in primary and secondary anti-OVA titers, inhibition of B16F10-OVA tumor growth, and improvement in survival (Figure 1a).

RESULTS AND DISCUSSION

Synthesis and Characterization of Ln-GAMP-NPs.

Lanthanide-AMP coordination nanoparticles (Ln-AMP-NPs), lanthanide-GMP coordination nanoparticles (Ln-GMP-NPs), and Ln-GAMP-NPs were prepared as described previously,²² based on the self-assembly of lanthanide ions and AMP, GMP, or AMP/GMP (1:1 M ratio) in aqueous solution. Sixteen of 17 rare-earth ions formed coordination nanoparticles with AMP, GMP, or AMP/GMP (Figure 1a and Figure S1). Promethium was not evaluated because it is radioactive. Scanning electron microscopy images of Ln-GAMP-NPs, europium-AMP coordination nanoparticles (Eu-AMP-NPs), and europium-GMP coordination nanoparticles (Eu-GMP-NPs) showed that these nanoparticles were ~20–30 nm in diameter (Figure S2). Eu-based nanoparticles were selected for elemental mapping by energy-dispersive X-ray spectroscopy and Fourier transform infrared spectroscopy. The results show the existence of Eu, C, N, P, and O in these nanoparticles (Figures 1b and S3). Zeta potential measurements showed that the surface charges of Ln-GAMP-NPs and Ln-GMP-NPs in water ranged from +3 to +18 mV, while those of Ln-AMP-NPs ranged from –3 to –11 mV (Figure S4).

Ln-GAMP-NPs Potently Activate IFN-I Responses in Raw 264.7-ISG Cells and THP-1-ISG Cells. We first evaluated the ability of the lanthanide coordination nanoparticles to stimulate an IFN-I response in mouse macrophages (Raw 264.7-ISG cells) and human monocytes (THP-1-ISG cells). First, the cytotoxicity of the nanoparticles was evaluated in both cell lines. The viability (in both cell lines) was more than 90% even at a nanoparticle concentration of 200 $\mu\text{g}/\text{mL}$, indicating negligible cytotoxicity (Figures S5 and S6). After incubation with various concentrations (50, 100, and 200 $\mu\text{g}/\text{mL}$) of these nanoparticles for different times (24, 48, and 72

h), only Ln-GAMP-NPs elicited strong IRF responses in Raw 264.7-ISG cells, and the IRF response depended on the incubation time and nanoparticle concentration (Figures 1c and S7 and S8). However, Ln-GMP-NPs and Ln-AMP-NPs did not elicit an IRF response, even at 200 $\mu\text{g}/\text{mL}$ and 72 h of incubation.

Moreover, a 1:1 mixture (w/w) of Ln-GMP-NPs and Ln-AMP-NPs did not elicit an IRF response at high concentrations or long incubation (Figures S9 and S10). Mixed solutions of LnCl_3 , GMP, AMP, or GMP + AMP (molar ratio 1:1) did not stimulate IRF responses, whereas free 2'3'-cGAMP, a positive control, elicited a strong concentration- and time-dependent response. More importantly, the solution prepared by mixing EuCl_3 solution with GMP + AMP solution in cell culture medium also did not elicit an IRF response in Raw 264.7-ISG cells, indicating that the Ln-GMAP-NP is required for activation of the STING pathway. A similar IRF response was observed in THP-1-ISG cells with Ln-GMAP-NPs (Figures 1d and S11 and S12), suggesting that Ln-GMAP-NPs can activate human STING *in vitro*. In addition, Ln-GAMP-NPs did not induce an obvious reporter signal in Raw-ISG STING-KO (KO = knockout) cells even at a concentration of 400 $\mu\text{g}/\text{mL}$, whereas the IFN- α/β protein induced a significant reporter signal in a concentration-dependent manner (Figures 1e and S13). These data confirm that Ln-GMAP-NPs can activate the STING pathway.

Eu-GAMP-NPs Induce Maturation of BMDCs via STING. We randomly selected Eu-based coordination nanoparticles (Eu-GAMP-NPs) to investigate their adjuvant effects on BMDCs. We first optimized Eu-GAMP-NPs by regulating the molar ratio of GMP/AMP from 10:1 to 1:10 and examined their ability to activate IRF responses in Raw 264.7-ISG and THP-1-ISG cells. Eu-GAMP-NPs with a GMP/AMP ratio of 1:1 induced the strongest IRF response among the five types of nanoparticles (Figure 2a). We attributed this response to more 2'3'-cGMAP analogues in the nanoparticles. After being stored at 4 °C for over 2 years, these Eu-GAMP-NPs still elicited the strongest IRF response among various nanoparticles (Figure 2b). A similar stimulatory IRF response to these Eu-GAMP-NPs was also observed in THP-1-ISG cells (Figure 2c, d), further confirming the optimal ratio and remarkable stability.

DCs, which are specialized antigen-presenting cells, are essential for antigen-induced adaptive immunity.²³ To facilitate antigen presentation, DCs must first mature by expressing costimulatory molecules and producing cytokines.²⁴ We next investigated the adjuvant effect of Eu-GAMP-NPs on the maturation of BMDCs. After 24 h of incubation with different Eu-GAMP-NPs, BMDCs treated with Eu-GAMP-NPs with a GMP/AMP ratio of 1:1 expressed significantly more CD80, CD83, and CD86 compared with control BMDCs (Figures 2e,f and S14). The increase in the expression of costimulatory molecules was comparable to that of 2'3'-cGAMP (a classic STING agonist). Note that STING-activated DCs also secrete more pro-inflammatory cytokines and type I interferons (IFNs).²¹ Compared with other treatments, the 1:1 ratio Eu-GAMP-NPs increased the production of tumor necrosis factor α (TNF- α) and interleukin 1 β (IL-1 β) in BMDCs by 5- to 10-fold and 3- to 5-fold, respectively (Figure 2g,h). Additionally, all treatments slightly increased IFN- α/β production in BMDCs (Figure S14). Collectively, the 1:1 ratio of Eu-GAMP-NPs showed stronger STING activation, leading to greater maturation of BMDCs. Therefore, we selected the 1:1

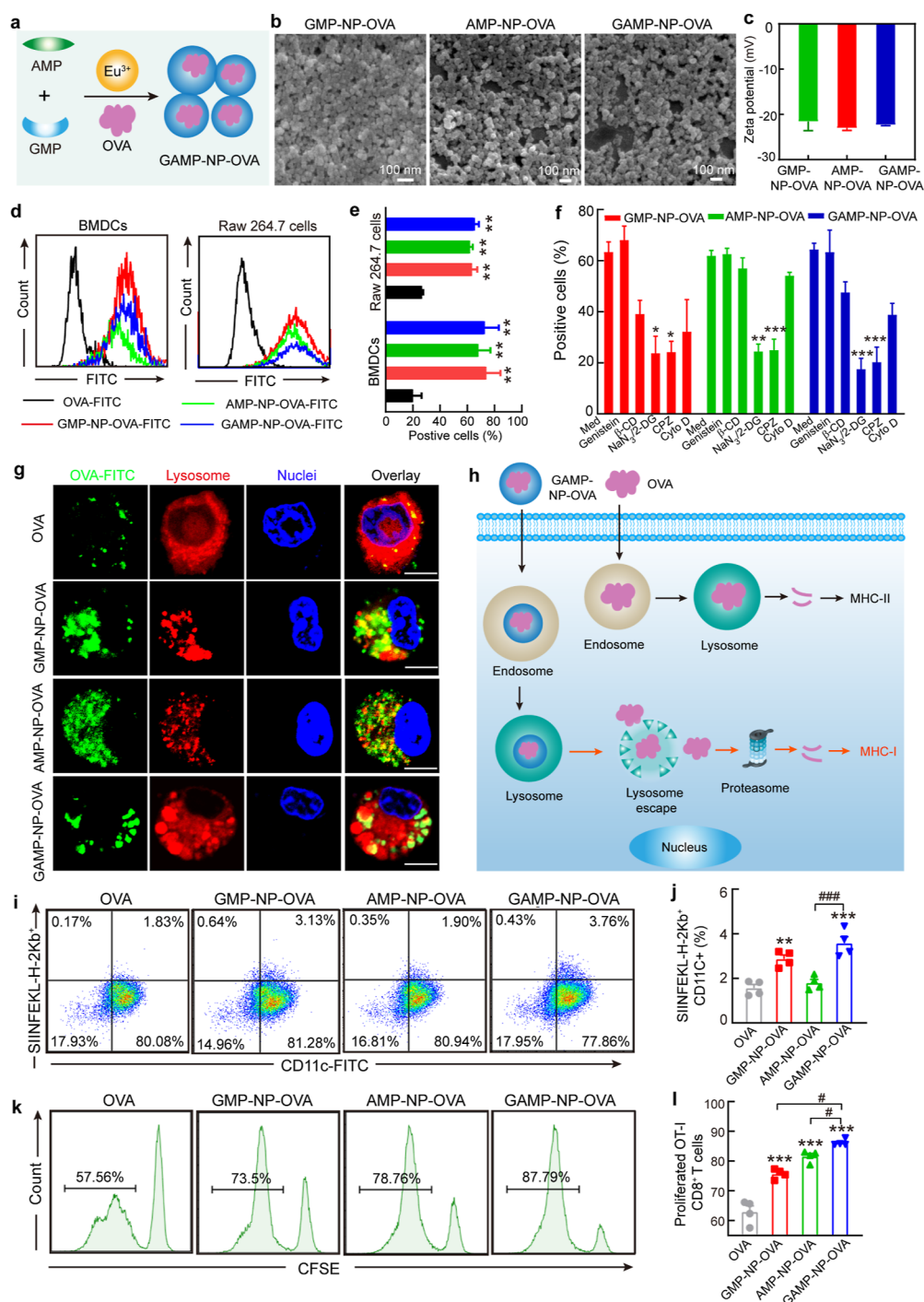


Figure 3. Eu-GAMP-NP-based vaccine promotes MHC class I antigen presentation. (a) Schematic of Eu-GAMP-NP-based vaccine preparation. (b) Scanning electron micrographs of nanovaccines. (c) Zeta potential of Eu-GAMP-NP-OVA in water measured by dynamic light scattering. (d, e) Effect of cellular antigen uptake of different nanovaccines on BMDCs and Raw 264.7 cells. (f) Investigation of the cellular uptake mechanism of BMDCs treated for 4 h with OVA-FITC or OVA-FITC encapsulated with Eu-GMP-NPs, Eu-AMP-NPs, or Eu-GAMP-NPs. Scale bar, 10 μ m. (g) Confocal imaging of BMDCs. (h) Schematic of the proposed mechanism of Eu-GAMP-NP promotion of antigen cross-presentation. (i, j) Flow cytometry plots and statistical data, showing OVA antigen cross-presentation efficiency in BMDCs treated with Eu-GMP-NP-OVA, Eu-AMP-NP-OVA, or Eu-GAMP-NP-OVA for 12 h. (k, l) Representative flow cytometric plots and statistical data, showing proliferation of OT-I CD3⁺CD8⁺ T cells after incubation with BMDCs pre-treated with different vaccines at a BMDC/T-cell ratio of 1:10. Values are means \pm s.e.m. ($n = 3-4$ biologically independent samples; asterisks: OVA-FITC (or OVA) vs other treatments, * $P < 0.05$; ** $P < 0.01$; hash: two different groups, # $P < 0.05$; ### $P < 0.001$; one-way ANOVA with Tukey's test).

ratio of Eu-GAMP-NPs (henceforth, GAMP-NPs) for further investigation.

Next, Eu-AMP-NPs (designated as AMP-NPs) and Eu-GMP-NPs (designated as GMP-NPs) were prepared for

comparison purposes. We first evaluated the adjuvant effects of GAMP-NPs, AMP-NPs, and GMP-NPs on the maturation of BMDCs. GAMP-NPs significantly stimulated the maturation of BMDCs by increasing the expression of DC maturation

markers (CD80, CD83, and CD86) by 1.5- to 2-fold (Figures 2i,j and S15) and the expression of cytokines such as TNF- α and IL-1 β by 4- to 8-fold (Figure 2k,l). In addition, only GAMP-NPs slightly enhanced IFN- α/β production in BMDCs (Figure S15). Next, EC₅₀ values for GAMP-NPs and cGAMP were measured in Raw 264.7-ISG cells at 23.06 and 13.72 $\mu\text{g}/\text{mL}$, respectively (Figure S16). Additionally, GAMP-NPs promoted the production of TNF- α and IL-6 by BMDCs in a concentration dependent manner (Figure S16), which might be related to the STING-activated proinflammation pathway. However, compared with cGAMP, GAMP-NPs significantly promoted IL-1 β production in a concentration-independent manner, indicating that GAMP-NPs may partially evoke inflammasome activation. In that regard, we mainly focus on the activated STING pathway.

To confirm the activation of the STING pathway, we evaluated the expression level of STING and its downstream markers, including phosphorylated STING (p-STING), IRF3, phosphorylated IRF3 (pIRF3), TBK1, and nuclear factor kappa-light-chain-enhancer of activated B cells (NF- κB) in macrophages by western blotting. Compared with other treatments, GAMP-NPs slightly promoted the expression of STING and p-STING and strongly increased the expression of pIRF3, NF- κB , and TBK1, indicating that GAMP-NPs activate the STING signaling pathway (Figures 2m and S17). Given that cGAMP can activate immune cells when bound to STING proteins in the ER,³ we speculate that GAMP-NPs, a 2'3'-cGAMP analogue, bind to STING and trigger an IRF3 type I-IFN signaling cascade (Figure S17).

To further investigate how GAMP-NPs activate the STING signaling pathway, molecular docking between GAMP-NPs and STING proteins was conducted. Based on titration calorimetry, energy-dispersive X-ray spectroscopy (Figures S18 and S19), and a previous report,²⁵ we hypothesize that the calculated molecular structure of Ln-GAMP-NPs allows relatively greater stability compared with the structures of Ln-GMP-NPs and Ln-AMP-NPs (Figure S20) because there is no aggregation of nucleotide molecules in Ln-GAMP-NPs. Note that each lanthanide ion can bind two nucleotide molecules, regardless of the size of the lanthanide.²⁶ To compare the structure of 2'3'-cGAMP for docking to STING proteins, we propose a simplified molecular structure of Ln-GAMP-NPs containing a lanthanide, GMP, and AMP (Figure 2n). Through dynamic molecular docking, Ln-GAMP-NPs can bind to the active site of mSTING^{R231} (ref 26) (Figure S21). In particular, the Ln-GAMP molecule forms 6 hydrogen bonds with chain A of mSTING, involving Arg²³⁷ and Thr²⁶⁶ and with chain B of mSTING, involving Thr²⁶², Ser²⁴⁰, Tyr²³⁹, and Arg²³⁷ (Figure 2o). Interestingly, Ln-GAMP-NPs closely resemble the binding of 2'3'-cGAMP, as shown by the superposition of the Ln-GAMP-bound mSTING cocrystal structure with the cGAMP-bound complex (Figure S21). Similar binding of Ln-GAMP-NPs was also obtained, when Ln-GAMP-NPs interacted with human STING^{R232} (ref 20) and a hSTING variant, hSTING-HAQ (ref 19a), by dynamic molecular docking (Figures S21 and S22). To verify this hypothesis, cellular thermal shift assay (CETSA) was conducted in Raw 264.7 cells. Similar to 2'3'-cGAMP, GAMP-NPs enhanced the stabilization of the STING protein with increasing temperature (Figure S23), indicating that GAMP-NPs directly interact with STING in Raw 264.7 cells.

GAMP-NPs Promote Antigen Uptake and MHC Class I Antigen Presentation. Given the potent effect of GAMP-

NPs on the maturation of BMDCs via STING, we next sought to evaluate their effect on antigen cross-presentation. To prepare GAMP-NP-based nanovaccines, ovalbumin (OVA), a model protein antigen, was encapsulated in coordination nanoparticles through self-assembly (Figure 3a). SEM images showed that the diameters of three nanovaccines based on coordination nanoparticles were approximately 20–30 nm (Figure 3b). Similar results were also found for 15 other lanthanide-based nanovaccine formulations (Figure S24). The surface charges of the three nanovaccines were close to -20 mV (Figure 3c), which can be attributed to the incorporation of negatively charged OVA. Next, the nanovaccine formulations were characterized by UV spectroscopy and fluorescence spectroscopy (Figure S25). When less than 0.5 mg of OVA was used, the loading efficacy of OVA was about 98%, suggesting high antigen encapsulation (Figure S25). Approximately, 80% of the loaded OVA was released from the three nanovaccines within 6 h. The cytotoxicity study showed that both Raw 264.7 and 3T3 cells were over 95% viable even at a high concentration of 400 $\mu\text{g}/\text{mL}$ of nanovaccines (Figure S25).

Antigen uptake by antigen-presenting cells, such as DCs or macrophages, is the first step for vaccine-induced adaptive immunity. Thus, we next evaluated the effect of GAMP-NPs on OVA uptake by BMDCs and macrophages. All three nanoparticles promoted OVA-FITC uptake ~ 3 -fold in BMDCs and 4-fold in Raw 264.7 cells (Figure 3d,e). Endocytosis inhibitor assays showed that the three nanovaccines were internalized by Raw 264.7 cells, mainly via clathrin-mediated endocytosis (Figures 3f and S26), suggesting that three kinds of nanovaccines remain in endosomes/lysosomes after uptake. After uptake by antigen-presenting cells, the intracellular localization of the antigen is closely associated with MHC cross-presentation pathways.²⁷ We next checked intracellular OVA localization using endosome/lysosome tracker staining. Most of the OVA-FITC delivered by these nanoparticles (over 80%) was not colocalized with lysosomes in BMDCs after 4 h, indicating efficient endosomal escape of the antigen (Figures 3g and S27). This enhancement of endosomal escape could be due to the pH response of the coordination nanoparticles.²⁸ We hypothesize that GAMP-NPs promote OVA escape from endosomes/lysosomes into the cytosol after enhancing OVA cellular uptake, effectively inducing MHC-I cross-presentation (Figure 3h). To verify this, we investigated whether these released cytosolic antigens could be effectively presented at the cell surface. Treatment of BMDCs with GAMP-NP–OVA for 24 h resulted in the highest concentrations of the SIINFEKL peptide on BMDC surfaces, as determined by staining SIINFEKL-H-2K^b complexes (Figure 3i,j). We also found that free OVA and AMP-NP-OVA-treated DCs exhibited weak surface presentation of the SIINFEKL epitope peptide after 24 h.

To study the effect of nanovaccines on DC-mediated MHC class I antigen presentation, BMDCs were treated with soluble OVA or nanoparticle-formulated OVA for 12 h. We then cocultured them with OT-I CD8⁺ T cells for 72 h and accessed the proliferation of OT-I CD8⁺ T cells. BMDCs pre-treated with GAMP-NP–OVA induced significant proliferation of OT-I CD8⁺ T cells, which was higher than that of BMDCs pretreated with other vaccine formulations (Figure 3k,l). The potent enhancement of antigen presentation by GAMP-NPs is mainly due to the fact that GAMP-NPs not only promote the escape of antigen endosomes but also enhance DC maturation compared with AMP-NPs and GMP-NPs. Meanwhile, CD8⁺ T

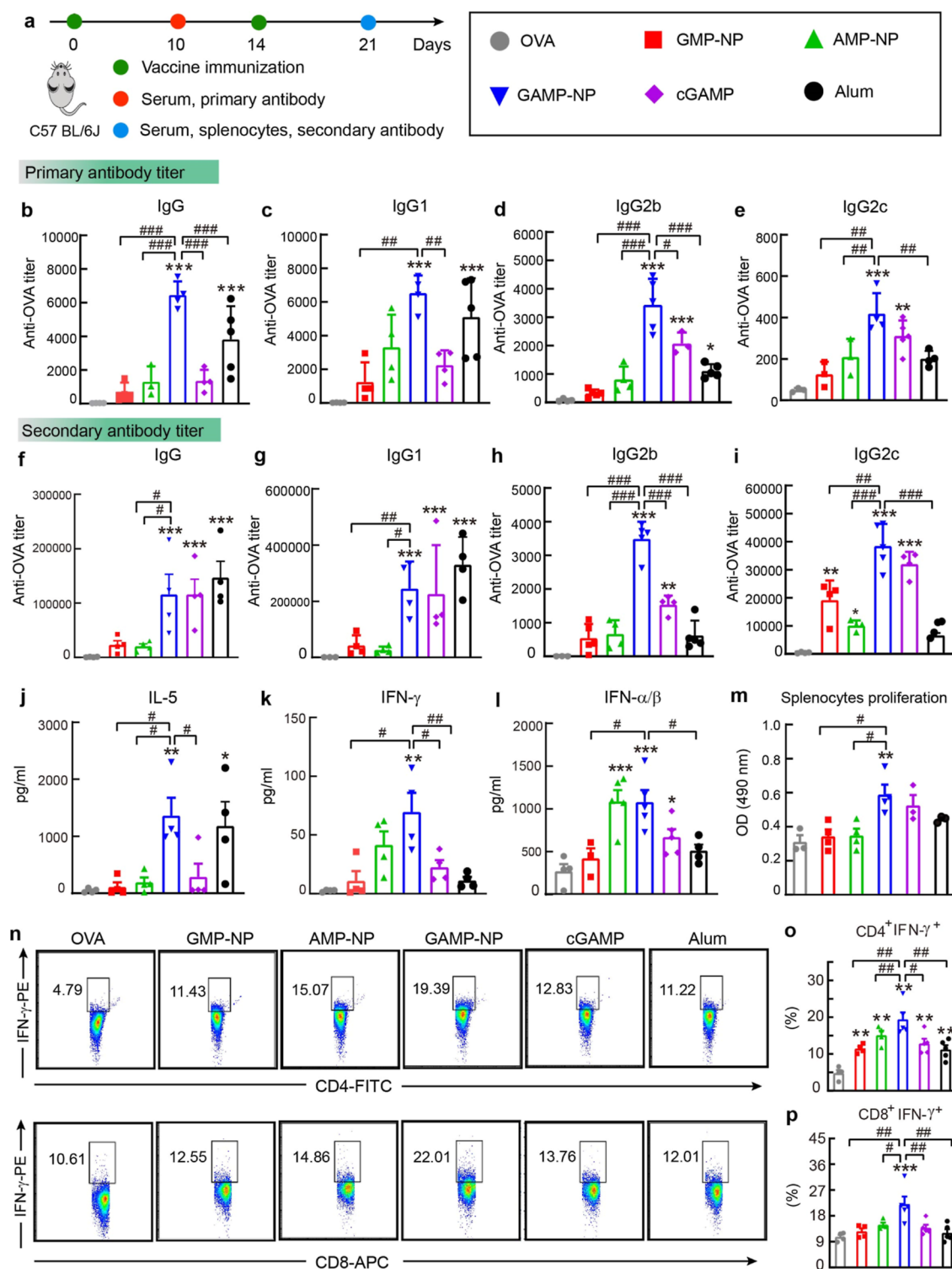


Figure 4. Eu-GAMP-NP–OVA induces a potent OVA-specific humoral immune response. (a) Scheme of vaccine immunization timepoints. (b–e) Production of anti-OVA, IgG1, IgG2b, and IgG2c, respectively, in plasma on day 10 after first immunization, measured using ELISA. (f–i) Secondary anti-OVA IgG, IgG1, IgG2b, and IgG2c titer, respectively, on day 21 after second immunization. (j–l) OVA-specific IL-5, IFN- γ , and IFN- α/β production in splenocyte supernatants, measured with an ELISA kit. (m) Ex vivo proliferation of splenocytes derived from mice immunized with different nanovaccines. (n–p) IFN- γ secreting CD4⁺ T cells (n and o) and CD8⁺ T cells (n and p) analyzed by flow cytometry in splenocytes after treatment with OVA ex vivo. T cells were defined as CD3⁺. All statistical data are shown as means \pm s.e.m. ($n = 4–5$ mice per group; asterisks: OVA vs other treatments, * $P < 0.05$; ** $P < 0.01$; *** $P < 0.001$; hash: two different groups, # $P < 0.05$; ## $P < 0.01$; ### $P < 0.001$; one-way ANOVA with Tukey’s test).

cells activated by GAMP-NP–OVA-pretreated BMDCs produced significantly higher amounts of TNF- α and IFN- γ than those activated by other treatments (Figure S28).

GAMP-NP–OVA Induces a Potent Humoral Immunity Supported by STING In Vivo. Lymph nodes are the primary immune organs where DCs present antigens to T cells,

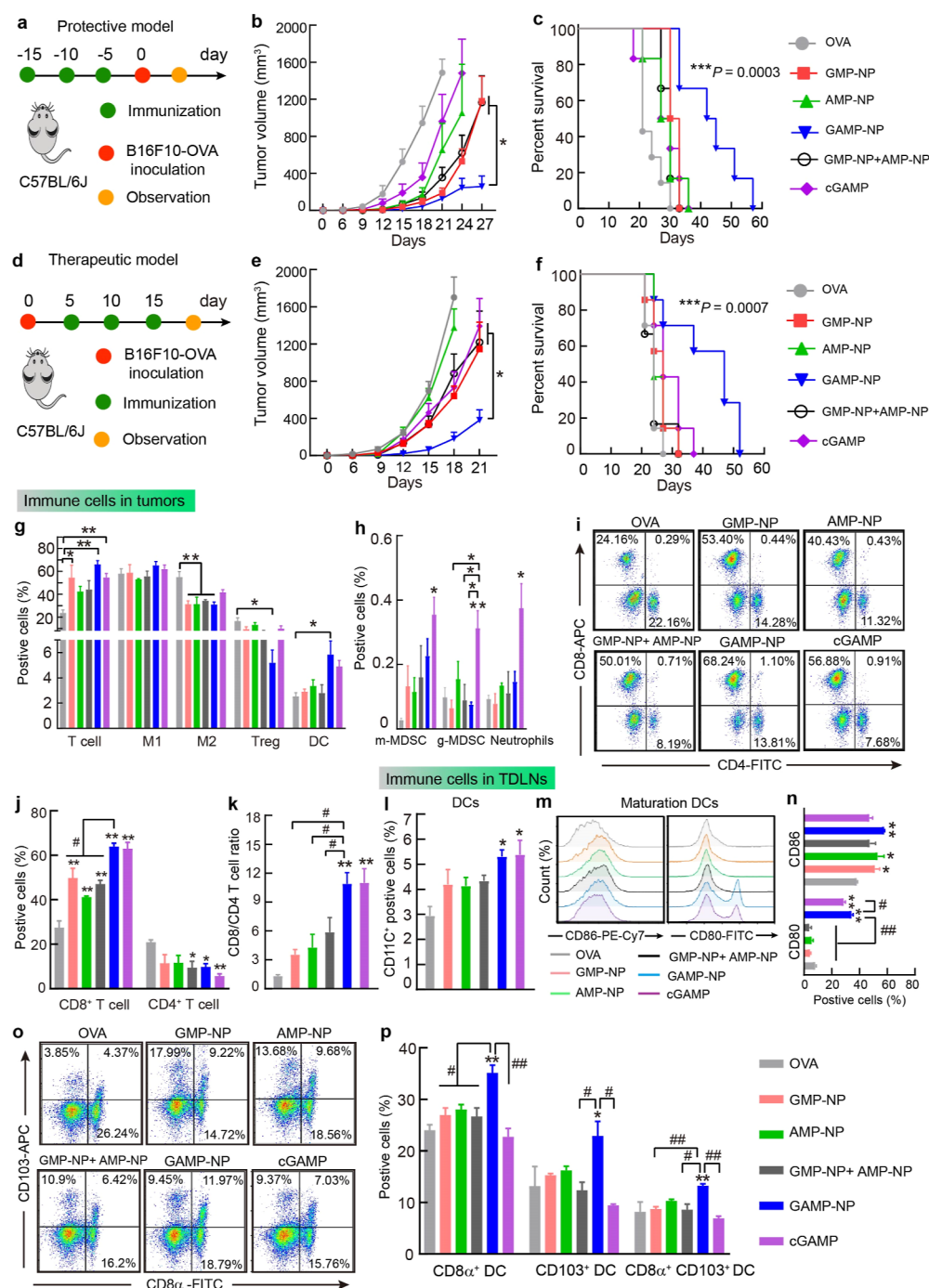


Figure 5. Eu-GAMP-NP-OVA inhibits tumor growth and prolongs survival in B16F10-OVA tumor-bearing mice. (a) Experimental design of the protective tumor challenge. (b,c) B16F10-OVA tumor growth curve and survival rate of mice in the protective model. (d) Experimental design of the therapeutic tumor challenge. (e,f) B16F10-OVA tumor growth curve and survival rate of mice in the therapeutic model. Data represent means \pm s.e.m. ($n = 6-7$ mice per group). (g-p) Eu-GAMP-NP-OVA shifts the immune cellular composition of the tumor microenvironment and tumor-draining lymph nodes. (g,h) Flow cytometric quantification of the proportion of T cells, M1 macrophages, M2 macrophages, Treg cells, DCs, m-MDSCs, g-MDSCs, and activated neutrophils in tumor tissues. (i,j) Flow cytometric plot and quantification of tumor-infiltrating CD4⁺ T and CD8⁺ T cells in tumor tissues. (k) Ratio of CD8⁺ T to CD4⁺ T cells in tumor tissues. (l-p) Different types of DCs in tumor-draining lymph nodes (TDLNs) analyzed using flow cytometry. (l) Flow cytometric quantification of the percentage of DCs in TDLNs. (m,n) Flow cytometric histogram and quantification of CD86 and CD80 expression by DCs (CD11c⁺) in TDLNs. (o,p) Flow cytometric plot and quantification of CD8α⁺ DC, CD103⁺ DC, or CD8α⁺ CD103⁺ DC in TDLNs. Data represent means \pm s.e.m. ($n = 4-5$ mice per group; asterisks: OVA vs other treatments, * $P < 0.05$; ** $P < 0.01$; hash: two different groups, # $P < 0.05$; ## $P < 0.01$; one-way ANOVA with Tukey's test).

triggering adaptive immune responses.²⁹ We evaluated the effect of GAMP-NPs on antigen transport to lymph nodes in vivo. GAMP-NPs promoted greater accumulation of OVA-FITC in lymph nodes 12 h after injection and retained more

OVA-FITC in lymph nodes than free OVA-FITC 48 h after injection (Figure S29). The highly efficient antigen transport to the lymph nodes might contribute to an antigen-specific immune response.

The adjuvant effect of GAMP-NPs on humoral immune response was further investigated in C57 BL/6J mice. The mice were subcutaneously injected with different coordination nanoparticle-based vaccines on day 0 and day 14 (Figure 4a). Primary and secondary anti-OVA antibodies in serum were detected by enzyme-linked immunosorbent assay (ELISA) on day 10 and day 21. For comparison, some mice were injected s.c. with OVA absorbed on aluminum (Alum), an adjuvant approved by the U.S. FDA for human vaccines. GAMP-NPs promoted anti-OVA IgG (IgG = immunoglobulin G) production by ~200-fold on day 10, compared with other treatments (soluble OVA) or even the commercial adjuvant (Alum) (~2-fold) (Figure 4b). This means that a vaccine-based GAMP-NPs could elicit a rapid, strong antigen-specific antibody response after a single vaccination. As with Alum, GAMP-NPs increased anti-OVA IgG1 by ~400-fold on day 10 compared with other treatments (soluble OVA) (Figure 4c). Moreover, GAMP-NPs increased primary anti-OVA IgG2b and IgG2c by 2–3 folds compared with other coordination nanoparticles (Figure 4d,e).

For secondary antibodies, GAMP-NPs increased anti-OVA IgG ~180-fold compared with soluble OVA. In addition, GAMP-NPs enhanced anti-OVA IgG by 6-fold and IgG1 by 9-fold compared with GMP-NPs and AMP-NPs, similar to free 2'3'-cGAMP and Alum (Figure 4f,g). Importantly, GAMP-NPs significantly increased secondary anti-OVA IgG 2b and IgG2c compared with other treatments (Figure 4h,i). Note that IgG1 and IgG2b/IgG2c isotypes are promoted by T helper type 2 (Th2) cytokines (e.g., IL-4/IL-5) and T helper Type 1 (Th1) cytokines (e.g., IFN- γ), respectively.³⁰ As with Alum, GAMP-NPs enhanced IL-5 production by 5- to 6-fold compared with the other two types of nanoparticles (Figure 4j), consistent with its effect on the IgG1 isotype. Unexpectedly, GAMP-NPs dramatically increased OVA-specific INF- γ production compared with other nanoparticles (Figure 4k), consistent with their effect on IgG2b and IgG2c isotypes. Since GAMP-NPs activate the STING pathway in vitro, we next evaluated their effect on production of STING pathway-associated cytokines, such as TNF- α and IFN- α/β , by splenocytes ex vivo. Notably, GAMP-NPs significantly increased the levels of TNF- α and IFN- α/β (Figures 4l and S30).

Because proliferation of T cells is one of the critical cellular functions after activation,³¹ we evaluated splenocyte proliferation ex vivo after re-stimulation with OVA. The GAMP-NP-based vaccine triggered dramatic proliferation of splenocytes compared with other treatments (Figure 4m). This proliferation enhancement was abolished when splenocytes were treated with bovine serum albumin (Figure S30), indicating OVA-specific proliferation. Note that after proliferation, T cells can rapidly eliminate target cells that express the same surface antigen by secreting cytokines such as IFN- γ . We next evaluated the effect of GAMP-NP-OVA on the induction of IFN- γ -secreting T cells. After the second stimulation with the antigen (OVA), the frequency of IFN- γ^+ CD4 $^+$ T cells (Th1 immune cells) was significantly increased in splenocytes of mice immunized with GAMP-NP-OVA (Figure 4n,o), consistent with the production of IgG2b and IgG2c isotypes. GAMP-NP-OVA significantly increased the ratio of IFN- γ^+ CD8 $^+$ T cells (cytotoxic T cells, CTL) (Figure 4n,p), indicative of a T cell-mediated cellular immune response. Notably, there were more activated CD4 $^+$ T cells (CD69 $^+$ CD4 $^+$) and CD8 $^+$ T cells (CD69 $^+$ CD8 $^+$) in the spleen cells of mice treated with

GAMP-NP-OVA than with other treatments (Figure S30), consistent with a previous study of systemic administration of SR-717 (a novel STING agonist).²⁰

For comparison, we also prepared a vaccine by mixing AMP-NP-OVA and GMP-NP-OVA (1:1, w/w). GAMP-NPs induced a more potent humoral immune response than the mixed vaccine (Figure S31). This suggests that mixing AMP-NPs and GMP-NPs is not related to an adjuvant effect related to activation of STING. To further confirm that co-encapsulation of antigen into nanoparticles is necessary to elicit the adjuvant effect, we mixed GAMP-NPs with OVA (GAMP-NPs + OVA) for further comparison. The mixed vaccine formulation still elicited a similar humoral immune response as the co-loading formulation (GAMP-NP-OVA) (Figure S32), confirming that the adjuvant effect of GAMP-NPs is independent of co-loading antigens. Note that activation of the STING signaling pathway is associated with the production of type-I IFNs (IFN- α/β), thereby promoting an effective CD8 $^+$ T cell immune response.² Considering the enhanced IFN- α/β production and CD8 $^+$ T cell activation with the GAMP-NP-OVA formulation, we conclude that the potent humoral immunity induced by GAMP-NP-OVA is indeed supported by the STING pathway.

GAMP-NP-OVA Induces Potent Cellular Immunity for Tumor Treatment. Given the enhanced IFN- γ production and CD8 $^+$ CTL activation by GAMP-NP-OVA, we hypothesized that GAMP-NP-OVA might be beneficial for tumor treatment. The antitumor effects of GAMP-NP-OVA were then examined in prophylactic and therapeutic B16F10-OVA models (Figure 5a,d). Mice injected with GAMP-NP-OVA had a smaller average tumor volume than other groups at all time points (Figure 5b), and their survival time was significantly prolonged (Figure 5c) mainly due to increased CD8 $^+$ CTL activation (Figure 4n, p). On the other hand, subcutaneous injection of the 2'3'-cGAMP/OVA formulation showed very little antitumor effect, although it elicited potent humoral immunity (Figure 3f). This also confirms that intratumoral injection of the small molecule 2'3'-cGAMP is essential for tumor growth inhibition. Similar to the prophylactic model, the GAMP-NP-based vaccine also significantly inhibited the tumor growth in the B16F10-OVA model, with 30% of animals still surviving at day 50 (Figure 5e,f), demonstrating the potential of GAMP-NP-OVA as a therapeutic cancer vaccine.

We next investigated the mechanism of tumor growth inhibition in tumor tissue and lymph nodes in the therapeutic B16F10-OVA model. GAMP-NP-based vaccine significantly increased the infiltration of T cells (CD3 $^+$) and DCs (CD11c $^+$) in the tumor tissue, which contribute to elicit adaptive immune responses (Figures 5g and S33). Moreover, GAMP-NP-OVA significantly decreased infiltration of M2 macrophages (CD206 $^+$ within CD11b $^+$ F4/80 $^+$ cells) and Treg cells (CD4 $^+$ CD25 $^+$ Foxp3 $^+$) (Figures S33 and S34), the two major immunosuppressive immune cells in the tumor microenvironment, suggesting that GAMP-NP-OVA repolarizes or recruits immune cells with reduced immunosuppressive capacity. To investigate the potential mechanism, we first examined the bio-distribution of GAMP-NP-OVA in tumor-bearing mice after s.c. immunization using ICP-OES (inductively coupled plasma optical emission spectroscopy). The results showed that Eu-GAMP-NP-OVA accumulated mainly in lymph nodes and partly in tumor tissues (Figure S35), resulting in a potent immune response or a partially varied microenvironment in the

tumor. In addition, 18 types of systemic cytokines and chemokines were detected in the serum of mice treated with GAMP-NP–OVA 4 h and 12 h after s.c. nanovaccine injection. There was no obvious change in serum levels of these cytokines and chemokines (Figure S35), indicating that the reshaped microenvironment of the tumor was caused by vaccination rather than systemic activation.

Subcutaneous administration of GAMP-NP–OVA showed little effect on two types of immunosuppressive cells, monocytic MDSCs (mMDSCs, $CD11b^+Ly6c^+Ly6g^-$) and granulocytic MDSCs (gMDSCs, $CD11b^+Ly6c^+Ly6g^+SSC^{high}$) (Figures 5h and S34). However, subcutaneous injection of a 2'3'-cGAMP-based vaccine increased the frequency of m-MDSCs and g-MDSCs (Figure 5h), resulting in a limited antitumor effect. Moreover, 2'3'-cGAMP/OVA increased the ratio of activated neutrophils ($CD11b^+Ly6c^+Ly6g^+SSC^{low}$) compared with free OVA (Figure 5h). All these results differ markedly from those of a previous study in which injection of 2'3'-cGAMP into the tumor showed no effect on those immune cells.¹⁰ This suggests that the injection routes of small molecule-STING agonists such as 2'3'-cGAMP may influence adjuvant effects.

GAMP-NP–OVA considerably increased $CD8^+$ T cell infiltration compared with other three nanoparticle-based vaccines (Figure 5i,j), consistent with a previous report attributing the antitumor effects of STING agonists primarily to activated $CD8^+$ T cells.²¹ Although there was a slight decrease in $CD4^+$ T cells in the tumor tissue of the GAMP-NP–OVA group, the $CD8^+/CD4^+$ T-cell ratio, a common prognostic indicator of immunotherapy and clinical success, was increased ~2-fold in the GAMP-NP–OVA group compared with other nanoparticle-based groups (Figure 5k).

We next investigated the effect of GAMP-NP–OVA on DC maturation in tumor-draining lymph nodes (TDLNs). Both GAMP-NP–OVA and 2'3'-cGAMP/OVA significantly promoted the accumulation of DC ($CD11c^+$) in TDLNs compared with other treatments (Figure 5l–n and Figure S36). However, GAMP-NP–OVA evoked DC maturation more potently than cGAMP/OVA, as shown by the greater enhancement in DC-maturation markers such as CD80. Note that $CD8a^+$ DC settlement in lymph nodes is critical for triggering a cytotoxic T lymphocyte (CTL) response that depends on STING-activated type-I IFN.³² In addition, $CD103^+$ DCs in lymph nodes can regulate the CTL response by controlling the migration, survival, and memory response of effector $CD8^+$ T cells.³³ Therefore, we evaluated the effect of GAMP-NP–OVA on $CD8a^+$ DCs and $CD103^+$ DCs in tumor-draining lymph nodes. $CD8a^+$ DCs were significantly increased in the TDLNs of the GAMP-NP–OVA group compared with those of other groups (Figure 5o,p), similar to a previous study.²¹ Moreover, GAMP-NP–OVA also enhanced the percentage of $CD103^+$ DCs and $CD8a^+ CD103^+$ DCs in TDLNs considerably more than other treatments, confirming a potent CTL immune response by GAMP-NP via Type-I IFN signaling. On the other hand, a free 2'3'-cGAMP-based vaccine showed little effect on these DCs in TDLNs (Figure 5o,p), further confirming the limitations of subcutaneous injection of 2'3'-cGAMP. In addition, multiple treatments with Eu-based nanovaccines did not induce body weight loss (Figure S37), and all treatments were well tolerated as demonstrated by serum chemistry (Figure S38). Histological analysis of the major organs removed from the mice under different treatments showed no abnormal histological conditions

(Figure S39), confirming the biocompatibility of Eu-GAMP-NPs.

CONCLUSIONS

In this study, we developed a series of simple, potent STING agonists (Ln-GAMP-NPs) by reacting lanthanide precursors with AMP/GMP solutions. Compared with 2'3'-cGAMP, the as-prepared Ln-GAMP-NP surrogate has many advantages, including simple preparation, low cost, high thermal and chemical stability, and no intratumoral administration. Moreover, unlike 2'3'-cGAMP, Eu-GAMP-NPs can function as a self-adjuvant platform to elicit systemic immune responses, while delivering antigens with a high loading efficiency.

Eu-GAMP-NPs significantly induce BMDC maturation via the STING pathway and promote MHC-I antigen presentation. Eu-GAMP-NP-based nanovaccines enhance primary and secondary anti-OVA IgG antibody responses and elicit $CD8^+$ CTL when injected subcutaneously. This suggests that such self-adjuvanted nanoparticles can be extended to the production of other types of vaccines, especially for recombinant protein-based vaccines such as COVID-19 vaccine.

This Eu-GAMP-NP-based vaccine significantly inhibits tumor growth and prolongs the life of tumor-bearing mice in both protective and therapeutic B16F10-OVA models. As for the immune mechanism, Eu-GAMP-NP–OVA induces an immunogenic tumor microenvironment by increasing immune-active cells and reducing immunosuppressive cells, associated with the STING-activating pathway. We speculate that these characteristics of Eu-GAMP-NPs will facilitate their use as a nano-delivery platform to deliver neoantigens for personalized therapy, nucleic acid-based vaccines for gene therapy, and drugs for combination therapy.

ASSOCIATED CONTENT

Supporting Information

The Supporting Information is available free of charge at <https://pubs.acs.org/doi/10.1021/jacs.2c03266>.

Materials and methods, detailed experimental procedures, preparation of nanoparticles, SEM images of nanoparticles, MTT assay of the cytotoxicity of nanoparticles, measurement of antibody titers, flow cytometry, energy-dispersive X-ray spectra, confocal images, and H&E staining images (PDF)

AUTHOR INFORMATION

Corresponding Authors

Changyang Gong – State Key Laboratory of Biotherapy and Cancer Center, West China Hospital, Sichuan University, Chengdu 610041, P. R. China; orcid.org/0000-0002-2913-0891; Email: chyong14@163.com

Xiaogang Liu – Department of Chemistry, National University of Singapore, Singapore 117543, Singapore; Agency for Science, Technology and Research, Institute of Materials Research and Engineering, Singapore 138634, Singapore; The N.1 Institute for Health, National University of Singapore, Singapore 117456, Singapore; orcid.org/0000-0003-2517-5790; Email: chmlx@nus.edu.sg

Authors

Zichao Luo – Department of Chemistry, National University of Singapore, Singapore 117543, Singapore

Xiuqi Liang – State Key Laboratory of Biotherapy and Cancer Center, West China Hospital, Sichuan University, Chengdu 610041, P. R. China

Tao He – State Key Laboratory of Biotherapy and Cancer Center, West China Hospital, Sichuan University, Chengdu 610041, P. R. China; orcid.org/0000-0002-6140-8179

Xian Qin – Department of Chemistry, National University of Singapore, Singapore 117543, Singapore

Xinchao Li – State Key Laboratory of Biotherapy and Cancer Center, West China Hospital, Sichuan University, Chengdu 610041, P. R. China

Yueshan Li – State Key Laboratory of Biotherapy and Cancer Center, West China Hospital, Sichuan University, Chengdu 610041, P. R. China; orcid.org/0000-0003-2343-1252

Lu Li – State Key Laboratory of Biotherapy and Cancer Center, West China Hospital, Sichuan University, Chengdu 610041, P. R. China

Xian Jun Loh – Agency for Science, Technology and Research, Institute of Materials Research and Engineering, Singapore 138634, Singapore; orcid.org/0000-0001-8118-6502

Complete contact information is available at:
<https://pubs.acs.org/10.1021/jacs.2c03266>

Author Contributions

¹Z.L. and X.L. contributed equally.

Notes

The authors declare no competing financial interest.

ACKNOWLEDGMENTS

This work was supported by the National Natural Science Foundation of China (82172094), Funds of Sichuan Province for Distinguished Young Scholars (2021JDJQ0037), and National Research Foundation, the Prime Minister's Office of Singapore under its NRF Investigatorship Programme (award no. NRF-NRFIO5-2019-0003). We acknowledge Z. Li and H. Bian for technical assistance. We thank Dr. X. Wu (Analytical and Testing Centre, Sichuan University) for his help with ICP-OES measurements.

REFERENCES

- (1) (a) Burdette, D. L.; Vance, R. E. STING and the innate immune response to nucleic acids in the cytosol. *Nat. Immunol.* **2013**, *14*, 19–26. (b) Sivick, K. E.; Desbien, A. L.; Glickman, L. H.; Reiner, G. L.; Corrales, L.; Surh, N. H.; Hudson, T. E.; Vu, U. T.; Francica, B. J.; Banda, T.; Katibah, G. E.; Kanne, D. B.; Leong, J. J.; Metchette, K.; Brumli, J. R.; Ndubaku, C. O.; McKenna, J. M.; Feng, Y.; Zheng, L.; Bender, S. L.; Cho, C. Y.; Leong, M. L.; van Elsas, A.; Dubensky, T. W.; McWhirter, S. M. Magnitude of therapeutic STING activation determines CD8⁺ T cell-mediated anti-tumor immunity. *Cell Rep.* **2018**, *25*, 3074–3085.
- (2) Corrales, L.; McWhirter, S. M.; Dubensky, T. W.; Gajewski, T. F. The host STING pathway at the interface of cancer and immunity. *J. Clin. Invest.* **2016**, *126*, 2404–2411.
- (3) Chen, Q.; Sun, L.; Chen, Z. J. Regulation and function of the cGAS-STING pathway of cytosolic DNA sensing. *Nat. Immunol.* **2016**, *17*, 1142–1149.
- (4) Barber, G. N. STING-dependent cytosolic DNA sensing pathways. *Trends Immunol.* **2014**, *35*, 88–93.
- (5) Barber, G. N. STING: infection, inflammation and cancer. *Nat. Rev. Immunol.* **2015**, *15*, 760–770.
- (6) (a) Luft, T.; Pang, K. C.; Thomas, E.; Hertzog, P.; Hart, D. N.; Trapani, J.; Cebon, J. Type I IFNs enhance the terminal differentiation of dendritic cells. *J. Immunol.* **1998**, *161*, 1947–1953. (b) Lorenzi, S.; Mattei, F.; Sistigu, A.; Bracci, L.; Spadaro, F.; Sanchez,

M.; Spada, M.; Belardelli, F.; Gabriele, L.; Schiavoni, G. Type I IFNs control antigen retention and survival of CD8⁺ dendritic cells after uptake of tumor apoptotic cells leading to cross-priming. *J. Immunol.* **2011**, *186*, S142–S150. (c) Martinez, J.; Huang, X.; Yang, Y. Direct action of type I IFN on NK cells is required for their activation in response to vaccinia viral infection in vivo. *J. Immunol.* **2008**, *180*, 1592–1597. (d) Spadaro, F.; Lapenta, C.; Donati, S.; Abalsamo, L.; Barnaba, V.; Belardelli, F.; Santini, S. M.; Ferrantini, M. IFN- α enhances cross-presentation in human dendritic cells by modulating antigen survival, endocytic routing, and processing. *Blood* **2012**, *119*, 1407–1417.

(7) Corrales, L.; Glickman, L. H.; McWhirter, S. M.; Kanne, D. B.; Sivick, K. E.; Katibah, G. E.; Woo, S.-R.; Lemmens, E.; Banda, T.; Leong, J. J.; Metchette, K.; Dubensky, T. W.; Gajewski, T. F. Direct activation of STING in the tumor microenvironment leads to potent and systemic tumor regression and immunity. *Cell Rep.* **2015**, *11*, 1018–1030.

(8) (a) Curran, E.; Chen, X.; Corrales, L.; Kline, D. E.; Dubensky, T. W., Jr; Dutttagupta, P.; Kortylewski, M.; Kline, J. STING pathway activation stimulates potent immunity against acute myeloid leukemia. *Cell Rep.* **2016**, *15*, 2357–2366. (b) Ohkuri, T.; Kosaka, A.; Ishibashi, K.; Kumai, T.; Hirata, Y.; Ohara, K.; Nagata, T.; Oikawa, K.; Aoki, N.; Harabuchi, Y.; Celis, E.; Kobayashi, H. Intratumoral administration of cGAMP transiently accumulates potent macrophages for anti-tumor immunity at a mouse tumor site. *Cancer Immunol. Immunother.* **2017**, *66*, 705–716.

(9) Dubensky, T. W., Jr; Kanne, D. B.; Leong, M. L. Rationale, progress and development of vaccines utilizing STING-activating cyclic dinucleotide adjuvants. *Ther. Adv. Vaccines* **2013**, *1*, 131–143.

(10) Shae, D.; Becker, K. W.; Christov, P.; Yun, D. S.; Lytton-Jean, A. K.; Sevimli, S.; Ascano, M.; Kelley, M.; Johnson, D. B.; Balko, J. M.; Wilson, J. T. Endosomolytic polymersomes increase the activity of cyclic dinucleotide STING agonists to enhance cancer immunotherapy. *Nat. Nanotechnol.* **2019**, *14*, 269–278.

(11) Chen, W.; KuoLee, R.; Yan, H. The potential of 3', 5'-cyclic diguanylic acid (c-di-GMP) as an effective vaccine adjuvant. *Vaccine* **2010**, *28*, 3080–3085.

(12) (a) Hobson, J.; Gummadidala, P.; Silverstrim, B.; Grier, D.; Bunn, J.; James, T.; Rincon, M. Acute inflammation induced by the biopsy of mouse mammary tumors promotes the development of metastasis. *Breast Cancer Res. Treat.* **2013**, *139*, 391–401. (b) Estourgie, S.; Nieweg, O.; Kroon, B. High incidence of in-transit metastases after sentinel node biopsy in patients with melanoma. *Br. J. Surg.* **2004**, *91*, 1370–1371.

(13) Lu, X.; Miao, L.; Gao, W.; Chen, Z.; McHugh, K. J.; Sun, Y.; Tochka, Z.; Tomasic, S.; Sadtler, K.; Hyacinthe, A.; Huang, Y.; Graf, T.; Hu, Q.; Sarmadi, M.; Langer, R.; Anderson, D. G.; Jaklenec, A. Engineered PLGA microparticles for long-term, pulsatile release of STING agonist for cancer immunotherapy. *Sci. Transl. Med.* **2020**, *12*, No. eaaz6606.

(14) (a) Benci, J. L.; Xu, B.; Qiu, Y.; Wu, T. J.; Dada, H.; Twyman-Saint Victor, C.; Cucolo, L.; Lee, D. S.; Pauken, K. E.; Huang, A. C.; Gangadhar, T. C.; Amaravadi, R. K.; Schuchter, L. M.; Feldman, M. D.; Ishwaran, H.; Vonderheide, R. H.; Maity, A.; Wherry, E. J.; Minn, A. J. Tumor interferon signaling regulates a multigenic resistance program to immune checkpoint blockade. *Cell* **2016**, *167*, 1540–1554. (b) Baird, J. R.; Friedman, D.; Cottam, B.; Dubensky, T. W.; Kanne, D. B.; Bambina, S.; Bahjat, K.; Crittenden, M. R.; Gough, M. J. Radiotherapy combined with novel STING-targeting oligonucleotides results in regression of established tumors. *Cancer Res.* **2016**, *76*, 50–61.

(15) (a) Brody, J. D.; Ai, W. Z.; Czerwinski, D. K.; Torchia, J. A.; Levy, M.; Advani, R. H.; Kim, Y. H.; Hoppe, R. T.; Knox, S. J.; Shin, L. K.; Wapnir, I.; Tibshirani, R. J.; Levy, R. In situ vaccination with a TLR9 agonist induces systemic lymphoma regression: a phase I/II study. *J. Clin. Oncol.* **2010**, *28*, 4324. (b) Liu, H.; Golji, J.; Brodeur, L. K.; Chung, F. S.; Chen, J. T.; deBeaumont, R. S.; Bullock, C. P.; Jones, M. D.; Kerr, G.; Li, L.; Rakiec, D. P.; Schlabach, M. R.; Sovath, S.; Growney, J. D.; Pagliarini, R. A.; Ruddy, D. A.; MacIsaac, K. D.; Korn,

- J. M.; McDonald, E. R. Tumor-derived IFN triggers chronic pathway agonism and sensitivity to ADAR loss. *Nat. Med.* **2019**, *25*, 95–102.
- (16) Hansen, N. M.; Ye, X.; Grube, B. J.; Giuliano, A. E. Manipulation of the primary breast tumor and the incidence of sentinel node metastases from invasive breast cancer. *Arch. Surg.* **2004**, *139*, 634–640.
- (17) (a) Koshy, S. T.; Cheung, A. S.; Gu, L.; Graveline, A. R.; Mooney, D. J. Liposomal delivery enhances immune activation by STING agonists for cancer immunotherapy. *Adv. Biosyst.* **2017**, *1*, 16000130. (b) Liu, Y.; Crowe, W. N.; Wang, L.; Lu, Y.; Petty, W. J.; Habib, A. A.; Zhao, D. An inhalable nanoparticulate STING agonist synergizes with radiotherapy to confer long-term control of lung metastases. *Nat. Commun.* **2019**, *10*, 5108.
- (18) (a) Park, K. S.; Xu, C.; Sun, X.; Louttit, C.; Moon, J. J. Improving STING agonist delivery for cancer immunotherapy using biodegradable mesoporous silica nanoparticles. *Adv. Ther.* **2020**, *3*, 2000130. (b) Chen, Y.-P.; Xu, L.; Tang, T.-W.; Chen, C.-H.; Zheng, Q.-H.; Liu, T.-P.; Mou, C.-Y.; Wu, C.-H.; Wu, S.-H. STING activator c-di-GMP-loaded mesoporous silica nanoparticles enhance immunotherapy against breast cancer. *ACS Appl. Mater. Interfaces* **2020**, *12*, 56741–56752.
- (19) (a) Pan, B.-S.; Perera, S. A.; Piesvaux, J. A.; Presland, J. P.; Schroeder, G. K.; Cumming, J. N.; Trotter, B. W.; Altman, M. D.; Buevich, A. V.; Cash, B.; Cemerski, S.; Chang, W.; Chen, Y.; Dandliker, P. J.; Feng, G.; Haidle, A.; Henderson, T.; Jewell, J.; Kariv, I.; Knemeyer, I.; Kopinja, J.; Lacey, B. M.; Laskey, J.; Lesburg, C. A.; Liang, R.; Long, B. J.; Lu, M.; Ma, Y.; Minnihan, E. C.; O'Donnell, G.; Otte, R.; Price, L.; Rakhilina, L.; Sauvagnat, B.; Sharma, S.; Tyagarajan, S.; Woo, H.; Wyss, D. F.; Xu, S.; Bennett, D. J.; Addona, G. H. An orally available non-nucleotide STING agonist with antitumor activity. *Science* **2020**, *369*, No. eaba6098. (b) Miao, L.; Li, L.; Huang, Y.; Delcassian, D.; Chahal, J.; Han, J.; Shi, Y.; Sadtler, K.; Gao, W.; Lin, J.; Doloff, J. C.; Langer, R.; Anderson, D. G. Delivery of mRNA vaccines with heterocyclic lipids increases antitumor efficacy by STING-mediated immune cell activation. *Nat. Biotechnol.* **2019**, *37*, 1174–1185. (c) Sun, X.; Zhang, Y.; Li, J.; Park, K. S.; Han, K.; Zhou, X.; Xu, Y.; Nam, J.; Xu, J.; Shi, X.; Wei, L.; Lei, Y. L.; Moon, J. J. Amplifying STING activation by cyclic dinucleotide-manganese particles for local and systemic cancer metalloimmunotherapy. *Nat. Nanotechnol.* **2021**, *16*, 1260–1270. (d) Li, S.; Luo, M.; Wang, Z.; Feng, Q.; Wilhelm, J.; Wang, X.; Li, W.; Wang, J.; Cholka, A.; Fu, Y.-x.; Sumer, B. D.; Yu, H.; Gao, J. Prolonged activation of innate immune pathways by a polyvalent STING agonist. *Nat. Biomed. Eng.* **2021**, *5*, 455–466.
- (20) Chin, E. N.; Yu, C.; Vartabedian, V. F.; Jia, Y.; Kumar, M.; Gamo, A. M.; Vernier, W.; Ali, S. H.; Kissai, M.; Lazar, D. C.; Nguyen, N.; Pereira, L. E.; Benish, B.; Woods, A. K.; Joseph, S. B.; Chu, A.; Johnson, K. A.; Sander, P. N.; Martínez-Peña, F.; Hampton, E. N.; Young, T. S.; Wolan, D. W.; Chatterjee, A. K.; Schultz, P. G.; Petrassi, H. M.; Teijaro, J. R.; Lairson, L. L. Antitumor activity of a systemic STING-activating non-nucleotide cGAMP mimetic. *Science* **2020**, *369*, 993–999.
- (21) Luo, M.; Wang, H.; Wang, Z.; Cai, H.; Lu, Z.; Li, Y.; Du, M.; Huang, G.; Wang, C.; Chen, X.; Porembka, M. R.; Lea, J.; Frankel, A. E.; Fu, Y.-X.; Chen, Z. J.; Gao, J. A STING-activating nanovaccine for cancer immunotherapy. *Nat. Nanotechnol.* **2017**, *12*, 648–654.
- (22) Nishiyabu, R.; Hashimoto, N.; Cho, T.; Watanabe, K.; Yasunaga, T.; Endo, A.; Kaneko, K.; Niidome, T.; Murata, M.; Adachi, C.; Katayama, Y.; Hashizume, M.; Kimizuka, N. Nanoparticles of adaptive supramolecular networks self-assembled from nucleotides and lanthanide ions. *J. Am. Chem. Soc.* **2009**, *131*, 2151–2158.
- (23) Wculek, S. K.; Cueto, F. J.; Mujal, A. M.; Melero, I.; Krummel, M. F.; Sancho, D. Dendritic cells in cancer immunology and immunotherapy. *Nat. Rev. Immunol.* **2020**, *20*, 7–24.
- (24) Palucka, K.; Banchereau, J. Cancer immunotherapy via dendritic cells. *Nat. Rev. Cancer* **2012**, *12*, 265–277.
- (25) Zhang, Z.; Morishita, K.; Lin, W. T. D.; Huang, P.-J. J.; Liu, J. Nucleotide coordination with 14 lanthanides studied by isothermal titration calorimetry. *Chin. Chem. Lett.* **2018**, *29*, 151–156.
- (26) Gao, P.; Ascano, M.; Zillinger, T.; Wang, W.; Dai, P.; Serganov, A. A.; Gaffney, B. L.; Shuman, S.; Jones, R. A.; Deng, L.; Hartmann, G.; Barchet, W.; Tuschl, T.; Patel, D. J. Structure-function analysis of STING activation by c [G (2', 5') pA (3', 5') p] and targeting by antiviral DMXAA. *Cell* **2013**, *154*, 748–762.
- (27) Joffre, O. P.; Segura, E.; Savina, A.; Amigorena, S. Cross-presentation by dendritic cells. *Nat. Rev. Immunol.* **2012**, *12*, 557–569.
- (28) Zheng, H.; Xing, L.; Cao, Y.; Che, S. Coordination bonding based pH-responsive drug delivery systems. *Coord. Chem. Rev.* **2013**, *257*, 1933–1944.
- (29) Schudel, A.; Francis, D. M.; Thomas, S. N. Material design for lymph node drug delivery. *Nat. Rev. Mater.* **2019**, *4*, 415–428.
- (30) Romagnani, S. Type 1 T helper and type 2 T helper cells: functions, regulation and role in protection and disease. *Int. J. Clin. Lab. Res.* **1992**, *21*, 152–158.
- (31) Farhood, B.; Najafi, M.; Mortezaee, K. CD8⁺ cytotoxic T lymphocytes in cancer immunotherapy: A review. *J. Cell. Physiol.* **2019**, *234*, 8509–8521.
- (32) (a) Gajewski, T. F.; Fuertes, M. B.; Woo, S.-R. Innate immune sensing of cancer: clues from an identified role for type I IFNs. *Cancer Immunol. Immunother.* **2012**, *61*, 1343–1347. (b) Hildner, K.; Edelson, B. T.; Purtha, W. E.; Diamond, M.; Matsushita, H.; Kohyama, M.; Calderon, B.; Schraml, B. U.; Unanue, E. R.; Diamond, M. S.; Schreiber, R. D.; Murphy, T. L.; Murphy, K. M. Batf3 deficiency reveals a critical role for CD8 α^+ dendritic cells in cytotoxic T cell immunity. *Science* **2008**, *322*, 1097–1100.
- (33) Ho, A. W.; Prabhu, N.; Betts, R. J.; Ge, M. Q.; Dai, X.; Hutchinson, P. E.; Lew, F. C.; Wong, K. L.; Hanson, B. J.; Macary, P. A.; Kemeny, D. M. Lung CD103⁺ dendritic cells efficiently transport influenza virus to the lymph node and load viral antigen onto MHC class I for presentation to CD8 T cells. *J. Immunol.* **2011**, *187*, 6011–6021.